Available online at www.sciencedirect.com
SCIENCE DIRECT®
Surface and Coatings Technology 183 (2004) 328–336
SURFACE & COATINGS TECHNOLOGY
www.elsevier.com/locate/surfcoat

Structure and tribological properties of WSe_x, WSe_x/TiN, WSe_x/TiCN and WSe_x/TiSiN coatings

D.V. Shtansky[a,*], T.A. Lobova[a], V.Yu. Fominski[b], S.A. Kulinich[a], I.V. Lyasotsky[c], M.I. Petrzhik[a], E.A. Levashov[a], J.J. Moore[d]

[a]*Moscow State Institute of Steel and Alloys, Leninsky pr. 4, 164, Moscow 119049, Russia*
[b]*Moscow State Engineering Institute, Kashirskoe sh. 31, Moscow 115409, Russia*
[c]*I.P. Bardin Central Research Institute for the Iron and Steel Industry, 2nd Baumanskaya Street, 9/23, Moscow 107005, Russia*
[d]*ACSEL Laboratory, Colorado School of Mines, Golden, CO 80401, USA*

Received 6 May 2003; accepted in revised form 5 September 2003

Abstract

WSe_x coatings were obtained by pulsed laser deposition (PLD) and ion-assisted PLD. The films were studied by means of X-ray diffraction, scanning and transmission electron microscopy, Auger electron spectroscopy and energy-dispersive X-ray spectroscopy. The WSe_x films were also characterized in terms of their hardness, elastic modulus, surface topography and wear performance. The structure of WSe_x films was shown to consist of various nanocrystalline mixtures of WSe_2 and W_3O phases in an amorphous WSe_x matrix. Depending on deposition conditions, the WSe_2 crystallites were oriented with their basal planes either parallel or perpendicular to the substrate surface. A correlation between an amount of W_3O phase and *c*-axis-oriented WSe_2 phase was outlined. The incorporation of oxygen atoms between the basal planes was shown to cause lattice distortion and resulted in anisotropy of the lattice parameter. Improved endurance of WSe_x coatings was due to their composite structure. The presence of hard underlayer, such as TiC, TiCN or TiSiN, was shown to be essential for extremely low friction coefficients down to 0.015–0.03. The WSe_x/TiC films showed low friction from the very start of the tests without initial maximum. The superior performance of WSe_x/TiSiN coatings both in air and under water suggests that the double-layer coatings are suitable for use in terrestrial tribological applications.

Keywords: Pulsed laser deposition; Ion-assisted PLD; WSe_x coatings; Structure; Friction; Wear

1. Introduction

Hard coatings based on carbides, nitrides and borides of transition metals provide superior mechanical and tribological properties. However, these coatings show a high coefficient of friction (0.85 TiB_2 [1], 0.8–0.9 TiC [2], 0.7–0.9 TiSiN [3]) and require lubricant to reduce friction. The friction of hard coatings can be improved by the deposition of a thin MoS_2 layer on top of the coatings [4]. Lubrication layer on the top of TiN reduces the friction, results in a low shear stress and leads to high bearing capacity [5]. The WS_x and MoS_x coatings are most widely studied. The pure metal dichalcogenide coatings have been reported to show friction coefficient down to 0.02 in vacuum [6]. Most sputter-deposited MoS_x films are substoichiometric ($1.1 < x < 2.0$) [7] and demonstrate low stability of friction coefficient [8]. Despite superior lubrication properties, WS_x and MoS_x coatings have limited application because of poor adhesion, limited performance in humid atmosphere, unstable friction coefficient, insufficient lifetime, porous columnar structure or wrong orientation for lubrication. In an attempt to improve their tribological performance, various approaches have been proposed focusing on densification of film structure to avoid the formation of voided, columnar structure; doping of metals which chemically bond with oxygen during the wear process; deposition of coatings with preferential orientation.

Oxygen contamination of MoS_x and WS_x affects their wear behavior. The tribological properties of metal dichalcogenides were reported to degrade in humid air;

*Corresponding author. Tel.: +7-095-230-4535; fax: +7-095-236-5298.
E-mail address: shtansky@shs.misis.ru (D.V. Shtansky).

0257-8972/04/$ - see front matter © 2003 Elsevier B.V. All rights reserved.
doi:10.1016/j.surfcoat.2003.09.047

Table 1
Basic PLD parameters and structure of the WSe_x films

No.	SHS target	Deposition temperature (°C)	Power density (J/cm^2)	W^+ ion energy (keV)	Phase composition
1	WSe_2	20	1.9	–	a-WSe_x, W_3O, $\perp WSe_2$, $\parallel WSe_2$ (traces)[a]
2		20	100	–	a-WSe_x, W_3O
3		250	1.9	–	$\perp WSe_2$, $\parallel WSe_2$, W_3O
4		250	100	–	a-WSe_x, $\perp WSe_2$, $\parallel WSe_2$, W_3O (traces)
5		20	1.9	30	$\parallel WSe_2 + W_3O$
6		20	100	10	$\parallel WSe_2 + W_3O$
7		20	100	30	a-$WSe_x + W_3O$ (traces)

[a] a-WSe_x denotes amorphous phase; $\perp WSe_2$ and $\parallel WSe_2$ denote in-plane and out-of-plane *c*-axis-oriented to the substrate surface WSe_2 crystallites, respectively.

therefore, pure MoS_2 and WS_2 are not suitable for use in terrestrial atmosphere. An interesting approach to improve the properties of coatings is to make a two-phase mixture of metal dichalcogenide with metal oxide that is believed to improve the lubrication and endurance of coatings.

Pulsed laser deposition (PLD) method has been successfully applied for the deposition of MoS_2 and WS_2 coatings [9–16]. The structure and chemical composition of coatings were shown to be very sensitive to the various process characteristics, such as ion energy, laser fluence, type of a buffer gas, etc. The bombardment of transition metal dichalcogenide films with high energy ions increases the density of coatings and improves their adhesion strength to substrate [17–19].

While the WS_x and MoS_x coatings have been studied quite intensively, a rather small amount of attention has been paid so far to the WSe_x coatings. Two compounds, WSe_2 and WSe_3, have been found in the W–Se system [20,21]. The stoichiometric range of WSe_2 phase has been shown to be very narrow, being of composition WSe_x, $1.97 < x < 2$ [22]. Recently, it has been reported that the addition of WSe_2 into MoS_x coating improves the endurance of self-lubricating coatings [23].

In the present study, WSe_x coatings were fabricated by PLD and ion-assisted PLD (IAPLD). The coatings were characterized in terms of their structure, chemical composition, crystallography and surface topography. The tribological behavior of IAPLD WSe_x coatings as well as double-layer WSe_x/TiC, WSe_x/TiCN and WSe_x/TiSiN coatings in pin-on-disk tests in various environments was studied.

2. Experimental

The WSe_2 target for PLD was manufactured by means of cold compacting technology under pressure of 600 MPa using WSe_2 powder obtained by self-propagating high-temperature synthesis (SHS). The WSe_2 powder was synthesized from W powder, 99.93% purity and particle size of 1–4 μm, and Se powder, 99.997% purity.

The tungsten diselenide films were deposited on various substrates by PLD technique described elsewhere [24] using WSe_2 target. Substrate materials included single crystal silicon (1 0 0), stainless steel (SS), high-speed steel (HSS) and hard alloy (HA). The diameter of the target was 20 mm and the thickness was 4 mm. The PLD system consisted of a 30-cm-diameter SS chamber with a target and a substrate holder, an electro-optically Q-switched Nd:yttrium–aluminum–garnet laser (wavelength 1.06 μm, laser pulse duration 10 ns) and a beam scanning and focusing system. The deposition experiments were fulfilled at energy density of 1.9 and 100 J/cm^2 and the substrate temperature was kept at 20 or 250 °C. The distance from the target to the substrate was 5 cm and the chamber was evacuated to obtain a pressure below 2.6×10^{-4} Pa. In order to improve adhesion between film and substrate in tribological tests the WSe_x films were also deposited by ion-assisted technique, wherein ions of the laser plume are accelerated to sufficiently high energy by a high-intensity, uniform electrostatic field [24]. High-energy ion bombardment was operating only at the initial stage of deposition. The ion energy was varied from 10 to 30 keV (Table 1) and the flux of ions was kept constant at 1.66×10^{12} ions/(cm^2 s).

For tribological tests, IAPLD WSe_x films were deposited over TiC, TiCN and TiSiN films on HA(TT8K6-type) substrate. The hard TiC, TiCN and TiSiN coatings were fabricated by DC magnetron sputtering (MS) of composite targets $TiC_{0.5}$, $Ti_5Si_3 + Ti$ and $Ti_5Si_3 + TiN$, respectively, in an atmosphere of argon or reactively (RMS), in a gaseous mixture of argon and nitrogen [25]. During deposition, the applied bias (U_{bias}) was controlled at −250 V and the substrate temperature was kept constant at 250 °C. The adhesion between hard film and substrate was improved by low energy ion bombardment of substrate at the initial stage of deposition using an additional Ar ion source operated at a fixed energy of 1.5 keV.

The microstructure and chemical composition of films were investigated by means of X-ray diffraction (XRD), Auger electron spectroscopy (AES), energy-dispersive

X-ray spectroscopy (EDS) and scanning and transmission electron microscopy (SEM and TEM). Thin foils for plain-view and cross-sectional TEM studies were prepared by conventional methods, which are described elsewhere [26]. The structure of the films was examined in a JEM-200CX (JEOL, Japan) TEM operating at 200 kV. The XRD spectra of films were obtained by a 'Geigerflex' X-ray diffractometer. The morphology and the thickness of the deposited films were determined in a JEOL field emission SEM (JSM-6700F, Japan). The surface topography and the root-mean-square roughness (R_{rms}) of as-deposited thin films were examined by scanning force microscopy (SFM, NanoScan, Russia [27]). The Auger analysis was performed in an LHS-10 SAM spectrometer.

The films were characterized in terms of their hardness (H), elastic modulus (E) and elastic recovery (W_e). The indentation hardness of the films was determined using a Nano Hardness Tester (CSM Instruments, Switzerland) equipped with a Berkovich diamond indentor tip, calibrated against fused silica. The hardness and Young's modulus were calculated using the Pharr and Oliver method [28]. The tribological properties of the coatings were evaluated using a conventional ball-on-disc tribometer (CSM Instruments, Switzerland) under a normal load of 5 N with a 3-mm diameter WC+6%Co ball as a counterpart material. Three tests were performed on each sample with wear track diameter varied within the range of 0.8–1.2 cm. Sliding speed was 10 cm/s.

3. Results and discussion

3.1. Target characterization

The SHS WSe_2 powder contained 54.0% W, 45.8% Se, 0.12% Fe, 0.01% Ni, 0.03% Cr, 0.015% Si and 0.036% Al. The size of the powder was 5–20 μm (Fig. 1a) and did not change during compacting process. The target was characterized by the presence of (0 0 0 1) preferential orientation. Fig. 1b shows the structure of WSe_2 grain in the target manufactured using SHS powder compacting process. The grains are defect-free and range from 3 to 20 μm.

3.2. Chemical composition

Rutherford backscattering spectroscopy was used to assess target composition. The Se/W ratio was of approximately 2 within the accuracy of 10%. Oxygen was also detected in an amount of 5–7 at.% by AES. The chemical composition of WSe_x films, as determined by EDS, however, was different from that of the target. The Se/W ratio in the films was shown to amount to 1:1; therefore, the films were enriched with W. The value of Se/W ratio in the films decreased further down

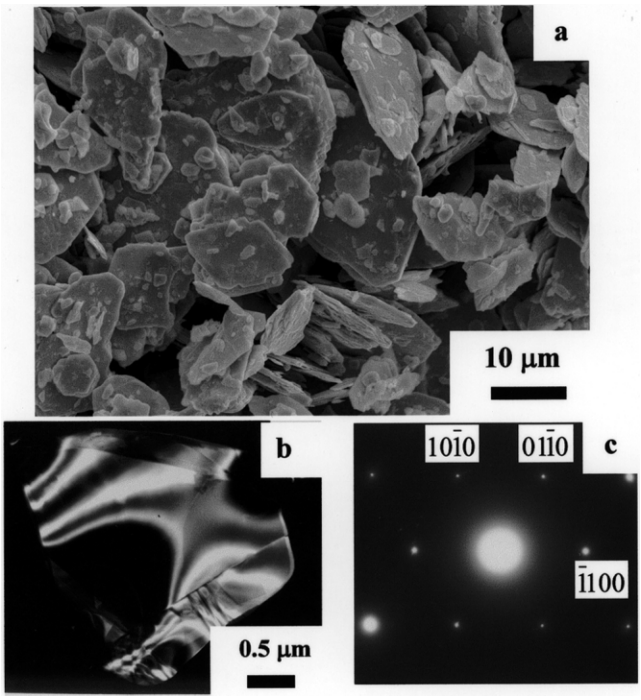

Fig. 1. (a) SEM micrograph of WSe_2 powder and (b) dark-field TEM micrograph of WSe_2 target showing a WSe_2 particle. (c) Selected area electron diffraction pattern from (b).

to 0.8 as the energy density was raised from 1.9 to 100 J/cm^2. This loss of Se can be explained by the scattering of light Se atoms through larger angles in comparison with heavier W atoms and re-evaporation of Se from the film surface. The presence of oxygen in the films was also confirmed and can be associated with oxygen atoms introduced either by the residual gas within the chamber or/and by being sputtered from the target.

3.3. Texture and lattice parameter

The results obtained show that most of WSe_2 crystallites were oriented with their c-axis either perpendicular or parallel to the substrate surface. Figs. 2 and 3 show the XRD spectra of WSe_x films deposited at 20 and 250 °C, respectively. For the film 1, two very broad reflections can be seen in the 6°–19° and 30°–50° 2θ ranges. The first broad reflection peaked at approximately 10.5°, as can be seen in the grazing incidence XRD (GIXRD) pattern at an incidence angle of 5° (Fig. 4). The scattering angle is much smaller than the position of (0 0 0 2) line for the stoichiometric WSe_2 phase (~15.9°). The shape and width of the reflections suggest that their origin is due to the presence of WSe_x phase in a poorly crystalline, quasi-amorphous state. Similar general features of the XRD patterns have also been interpreted by other groups as disorder effects induced by randomly stacked basal planes with fluctuation of the distance between them [29,30]. The XRD

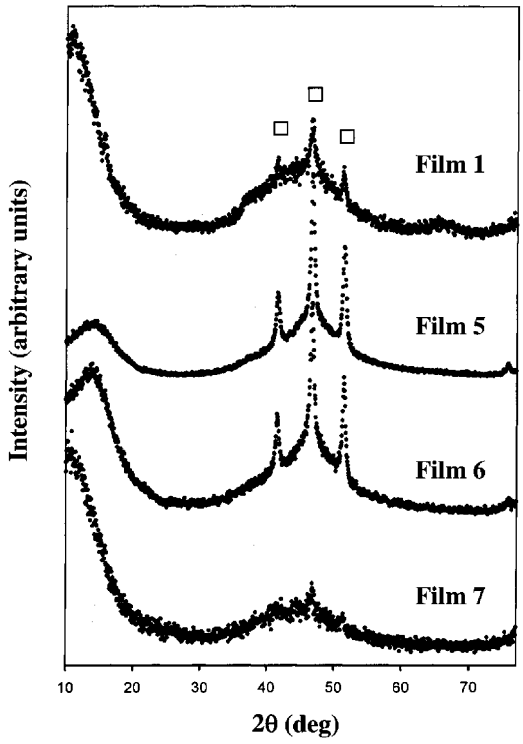

Fig. 2. XRD spectra of WSe_x films deposited at $T=20$ °C. W_3O reflections (□).

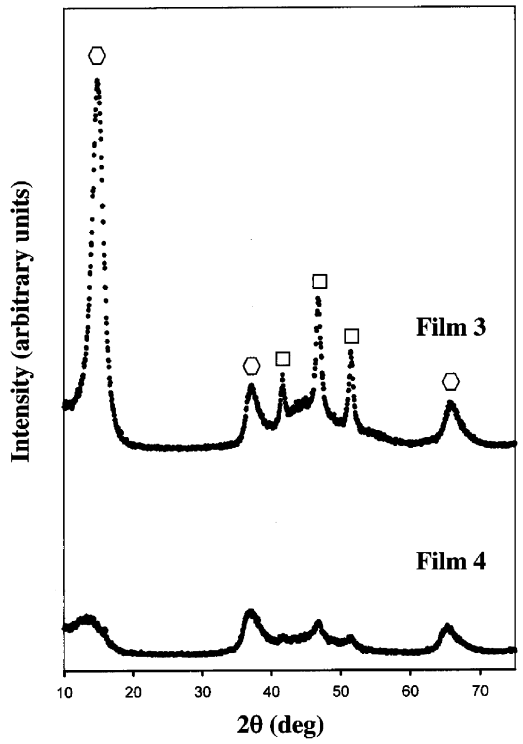

Fig. 3. XRD spectra of WSe_x films deposited at $T=250$ °C. W_3O reflections (□); WSe_2 reflections (⬡).

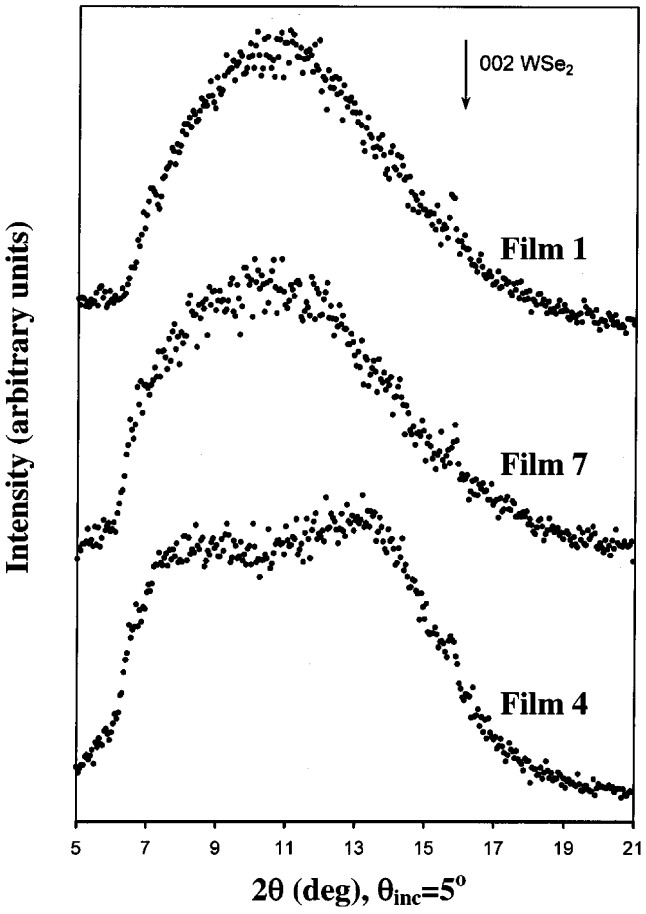

Fig. 4. GIXRD patterns at an incidence angle of 5° showing the first broad reflection in the range of 6–19° 2θ.

spectrum of the film 1 did not reveal (0 0 0 2) reflection of WSe_2 phase, whereas several reflections from the (0 0 0 2), (0 0 0 4) and (1 0 $\bar{1}$ 0) planes of WSe_2 phase were visible on the selected-area electron diffraction (SAED) pattern (Fig. 5a). This indicates the presence of a strong texture, the WSe_2 (0 0 0 1) basal planes being perpendicular to the substrate surface (hereafter, referred as $\perp WSe_2$ phase). Three peaks from the (0 0 2), (0 1 2) and (1 1 2) lattice planes of W_3O phase can be distinguished upon the background of the second broad peak suggesting the co-existence of crystalline W_3O and amorphous WSe_x(a-WSe_x) phases. This analysis shows that the structure of the film 1 consists of a mixture of WSe_2 phase with an edge-plane preferred orientation, randomly redistributed W_3O phase and quasi-amorphous WSe_x phase (Figs. 2 and 5). The results presented here are the first experimental observation showing that WSe_x films are multicomponent and consist of a mixture of three phases.

The XRD patterns of the films 1 (Fig. 2) and 2 (not shown) were similar. In contrast, an analysis of the film 2 by SAED did not reveal any noticeable reflections belonging to crystalline WSe_2 phase except (0 0 0 2)

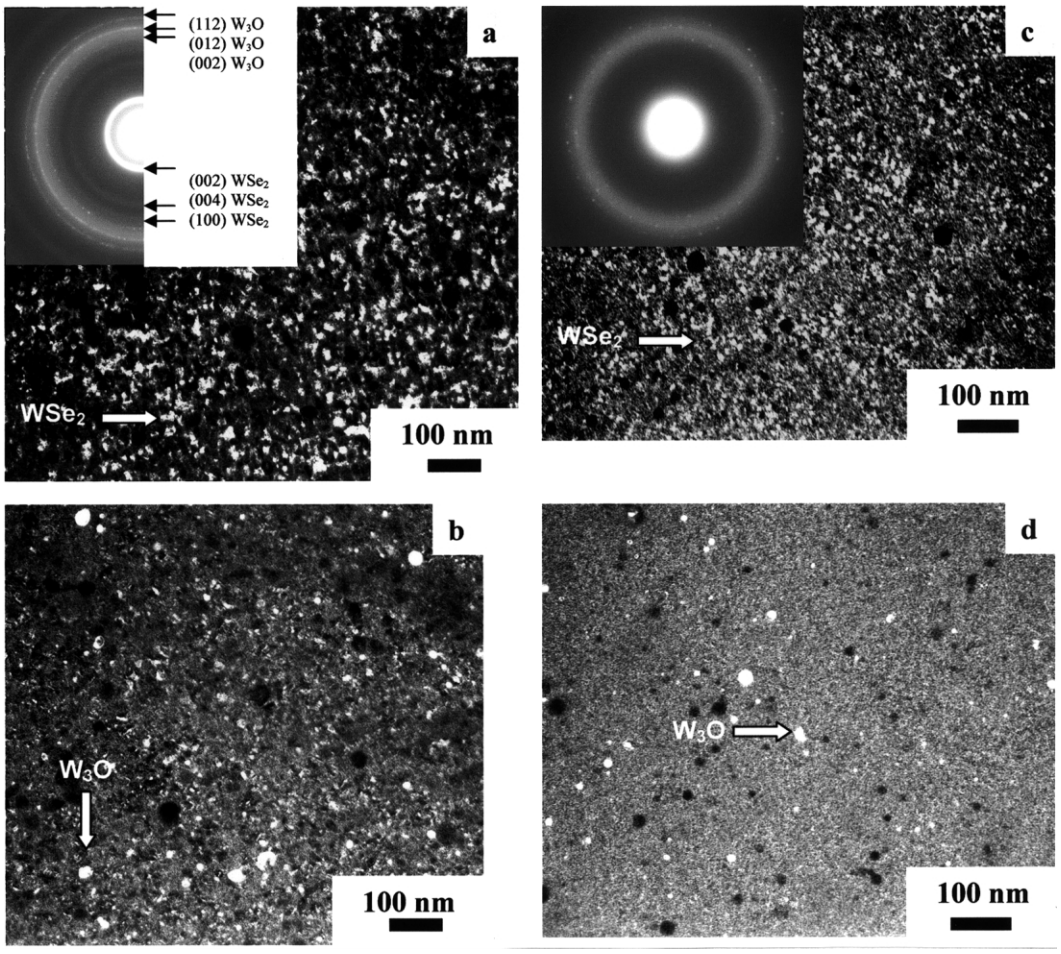

Fig. 5. Dark-field TEM micrographs (plain-view) of WSe_x films formed from parts of the (a), (c) $(0\,0\,0\,2)_{WSe_2}$ and (b), (d) $(0\,1\,2)_{W_3O}$ diffraction rings. (a), (b) film 1; (c), (d) film 2.

line which is weak and diffuse. This result implies that the basal planes in the film 2 are roughly parallel to each other but randomly rotating about the layer normal, similar to the turbostratic BN [31]. The WSe_2 phase has short-range order limited to the small particles (Fig. 5c) consisting of stacking faults parallel to the basal planes. The particle orientation is not random, but such that the basal planes are mostly perpendicular to the substrate surface. Therefore, $\perp WSe_2$ phase in the film 2 presents an intermediate case between a purely random network and crystalline WSe_2 phase. Thus, when laser fluence was increased to 100 J/cm^2, the amount of crystalline $\perp WSe_2$ phase decreased drastically, while the volume fraction of quasi-amorphous phase WSe_2 increased (Table 1).

The film 3, deposited at higher temperature $T=250$ °C and $P=1.9$ J/cm^2, was characterized by the presence of a strong (0 0 0 2) peak from the WSe_2 phase (referred as $\parallel WSe_2$ phase) indicating that the film was highly textured with [0 0 0 1] axis normal to the Si substrate (Fig. 3). The peak position corresponds to a spacing of approximately 0.66 nm, which is consistent with powder spectrum of WSe_2 phase (card No. 38-1388, JCPDS). The SAED pattern revealed diffraction lines (0 0 0 2), (0 0 0 4), $(1\,0\,\bar{1}\,0)$, $(1\,0\,\bar{1}\,3)$, $(1\,1\,2\,\bar{0})$ and (0 0 0 8) from WSe_2 phase. The (0 0 0 2) peak in the SAED pattern is the strongest one compared with the other peaks that are weak and diffuse. Thus, the combination of XRD and SAED results suggests that nearly all crystallites are oriented by such a way that their basal planes are either parallel or perpendicular to the substrate surface (Table 1). This is in agreement with the experimental data by Pouzet et al. [32], who reported on the mixed orientation due to competitive growth of WSe_2 crystallites $(0\,0\,0\,1)\parallel(1\,0\,0)$Si and $(0\,0\,0\,1)\perp(1\,0\,0)$Si.

With increasing power density up to 100 J/cm^2, the intensity of (0 0 0 2) peak decreased and its position shifted to lower diffraction angles (Fig. 3, film 4). This might be attributed to extension of the structure in the *c*-direction due to disorder effects, similar to the previous results [33]. Note that the low 2θ XRD peak from some dichalcogenide films grown by ion-beam-assisted depo-

sition, similar to that observed in Fig. 4, has been reported by Seitzman et al. [34] and ascribed to a local interplanar expansion of the crystal structure normal to basal planes [33].

IAPLD films 5 and 6 also exhibit the pronounced (0 0 0 2) peak of WSe_2 phase indicating strong planar (0 0 0 1) preferential orientation (Fig. 2). In these particular cases an amount of WSe_2 phase with edge-plane texture and amorphous phase was quite small. Therefore, the structure of films 5 and 6 may be interpreted as a mixture of (0 0 0 1)-oriented WSe_2 and W_3O phases.

A strong correlation between an amount of W_3O and $(0\,0\,0\,1)\|(1\,0\,0)_{Si}$-oriented WSe_2 phases was found. The growth of $\|WSe_2$ phase is accompanied by increase of volume fraction of W_3O phase. This phenomenon can be understood by comparison of the lattice parameters of the $\|WSe_2$ and $\perp WSe_2$ phases. The value of lattice parameter of $\perp WSe_2$ phase calculated on the basis of the planes (0 0 0 2), (0 0 0 4) and (0 0 0 8) in SAED pattern was correspondingly higher than that from the $(1\,0\,\bar{1}\,0)$ and $(1\,0\,\bar{1}\,3)$ lines. This is a clear indication of an anisotropy of the lattice parameter in $(0\,0\,0\,1)\perp(1\,0\,0)_{Si}$-oriented WSe_2 phase. The lattice parameter of $\|WSe_2$ phase derived from the (0 0 0 2) XRD reflection was, however, close to that of the bulk WSe_2 specimen. We believe that the distortion was probably caused by the incorporation of oxygen atoms between the basal planes that grew normal to the substrate surface. The penetration of light atoms (oxygen, alkali metals) between the basal planes of layered metal dichalcogenides has previously been reported [35,36]. In the case of WSe_2 crystallites growing by such a way that $(0\,0\,0\,1)\|(1\,0\,0)_{Si}$, a phase separation WSe_2+W_3O occurs and an amount of amorphous phase decreases. Therefore, one can expect that phase separation could correlate with the disordered state.

3.4. Structure and phase composition

A combination of XRD and TEM techniques has enabled the identification of the phase composition of WSe_x films. The typical plain-view dark-field TEM micrographs and corresponding SAED patterns of as-deposited WSe_x films are shown in Fig. 5. All films consisted of WSe_x crystallites, 2–30 nm in size, with different preferred orientations depending on deposition conditions, randomly oriented W_3O crystallites, 15–100 nm in size, and a-WSe_x phase. When irradiation density was increased, the WSe_2 grain size slightly decreased from 5–30 to 2–20 nm (Fig. 5a and c), whereas the average crystallite size of W_3O phase did not change. All the diffraction lines in the SAED patterns were identified as belonging to either hexagonal WSe_2 phase or cubic phase A15 type based on W_3O (card No. 41-1230, JCPDS) and no additional lines were observed.

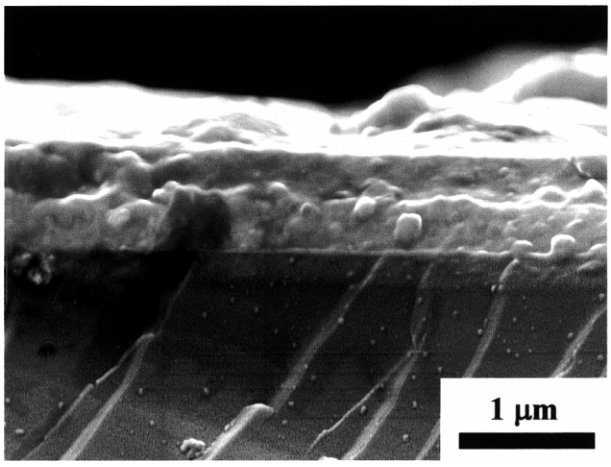

Fig. 6. SEM micrograph of WSe_x film 1. Cross-sectional specimen was sputter-coated with 2-nm-thick Au prior to analysis.

In the present study, the qualitative element analysis of the W_3O crystallites and the surrounding matrix in thin foils was carried out in the TEM mode. The results of the EDS analysis showed that Se content in the W_3O particles is negligible in comparison with that in the matrix confirming formation of tungsten oxide, which is in agreement with the XRD.

3.5. Film morphology and surface topography

The SEM cross-section fracture of the WSe_x film 1, 0.75 μm thick, revealed a columnless morphology (Fig. 6). The film is dense but has large spherical inclusions, 0.2–0.3 μm in size. The accumulation of spherical particles into the growing MoS_x films deposited at high energy density was also reported previously [11].

Data from EDS (Fig. 7) and TEM analyses showed that the structure and chemical composition within the large spherical particles in the film is identical to that within the surrounding matrix. Therefore, it is proposed that these spherical particles crystallized from melt. The SFM image in Fig. 8 shows that the surface of the film is covered with fully developed 3D islands with the size varying within the range of 70–250 nm ($R_{rms}=20$ nm for a 5×5 μm^2 scan area). The size of 3D hills on the film surface is larger than the crystallite size; therefore, one dome-like hillock on the film surface consists of several grains.

3.6. Mechanical and tribological properties

The hardness of WSe_x films was of approximately 5.2 ± 0.8 GPa, that is, higher than the 2–3 GPa hardness of typical solid lubricants [37]. The hardness value is, however, close to that of 4.7 GPa for MoS_2 coating [38]. The increase in hardness is believed to be due to

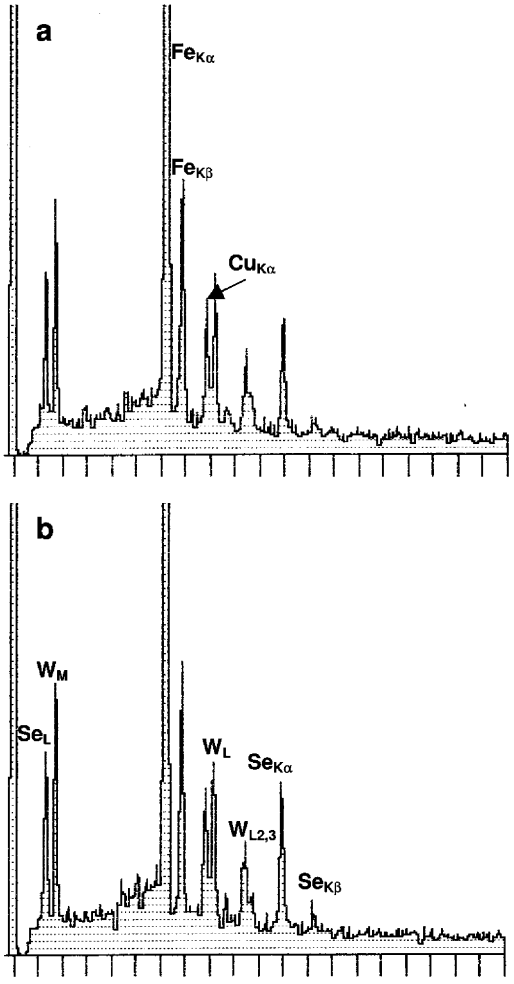

Fig. 7. EDS spectra of WSe_x film 1 taken from (a) the large spherical particle in the film, 0.3 μm in size, and (b) the surrounding matrix. The film was deposited on SS substrate.

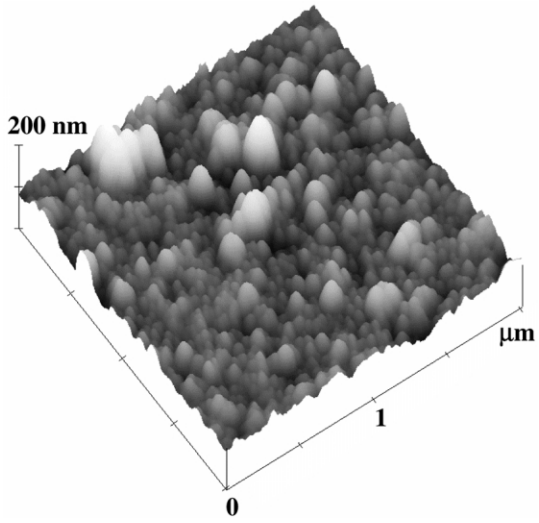

Fig. 8. SFM surface image of WSe_x film 1.

the presence of metal oxide particles. The Young's modulus changed within the range of 90–110 GPa.

The friction coefficient of IAPLD WSe_x films deposited on HSS substrate vs. hard alloy was found to be very low and changed within the range of 0.04–0.12 depending on the deposition conditions (Fig. 9). The difference in friction can be attributed to the higher volume fraction of *c*-axis-oriented WSe_2 phase in the film 6 in comparison with the film 5. Films tested at a low load of 1 N showed longer lifetime than those tested at 5 N.

For friction tests, thin WSe_x films were also deposited on the top of the hard coatings, such as TiC, TiCN or TiSiN. The values of hardness, Young's modulus, friction coefficient and wear rate of the hard films are presented in Table 2. The IAPLD WSe_x/hard coatings were tested for wear resistance at a normal load of 5 N

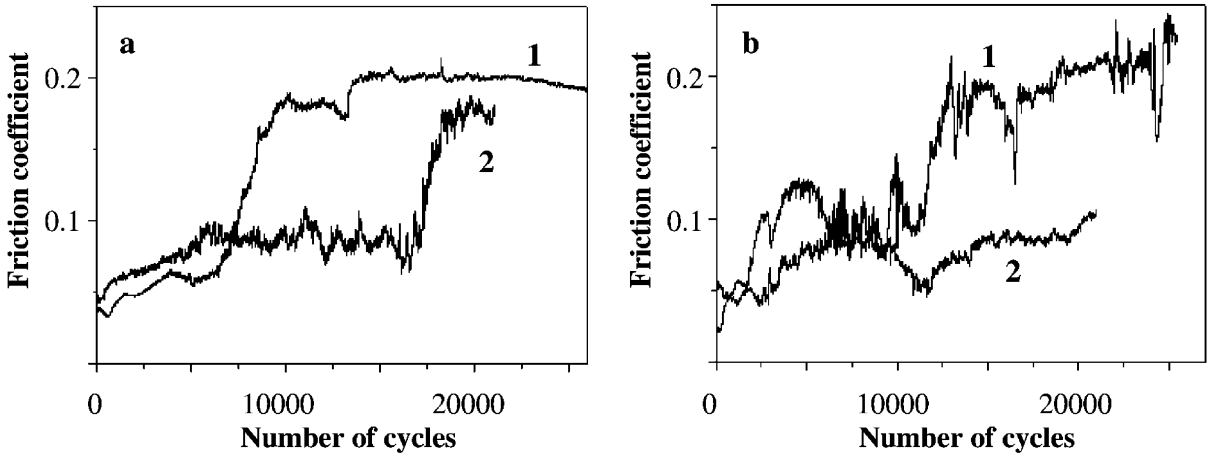

Fig. 9. Friction coefficient of WSe_x films deposited by IAPLD on HSS substrate against 3-mm WC + 6%Co ball at a load of 1–5 and 2–1 N. (a) Film 6; (b) film 5.

Table 2
Hardness, Young's modulus, friction coefficient and wear rate of the TiC, TiCN and TiSiN films

	TiC	TiCN	TiSiN
Hardness, H (GPa)	30 ± 3	21 ± 3	28 ± 2
Young's modulus, E (GPa)	445 ± 60	234 ± 20	320 ± 20
Friction coefficient, μ	0.21	0.17	0.5–0.6
Wear rate, V_w (10^{-7} mm^3 N^{-1} m^{-1})	9.6	9.8	12–14

(contact pressure approximately 2.8 GPa) and sliding speed of 10 cm/s, where the WSe_x films survived for 8000 cycles. It was frequently reported that the film is in wrong orientation for lubrication if the basal planes are perpendicular to the substrate [39]. Therefore, the film 5 was chosen as a self-lubricating layer due to its strong *c*-axis [0 0 0 1] texture. The self-lubricating layer of WSe_x/TiCN coating did not wear through over the total sliding distance of 1000 m (~19 500 cycles). The friction coefficient varied between 0.04 and 0.015 at 30% humidity depending on the type of supporting coating. Fig. 10 shows the friction coefficients of the WSe_x/TiC, WSe_x/TiCN and WSe_x/TiSiN coatings against 3 mm WC+6%Co ball as a counterpart material. The WSe_x films, 0.6–0.7 μm thick, were deposited by IAPLD on HSS substrates. The thickness of hard underlayer deposited by MS or RMS was varied within the range of 0.7–0.9 μm. The friction coefficient of WSe_x/TiCN and WSe_x/TiSiN coatings displayed an initial maximum, 0.07 in height, followed by a drop to 0.03 after 300 m (WSe_x/TiCN) and 0.015 after 250 m (WSe_x/TiSiN). The appearance of initial maximum has been reported for TiN–MoS_2 coatings to be attributed to the formation of oxide transfer film based on rutile [40]. No such maximum was observed in the case of WSe_x/TiC coating, indicating that the contact adhesion was lower. Wear-through of the top layer of WSe_x/TiC and WSe_x/TiSiN coatings occurred after approximately 7500 cycles, whereas coefficient of friction of WSe_x/TiCN coating remained below 0.05 after 20 000 revolutions. The friction coefficient of double-layered coatings in atmospheric conditions was an order of magnitude lower than that of carbide, nitride and carbonitride coatings.

It was frequently reported on friction induced re-orientation of MoS_2 and WS_2 basal planes parallel to substrate surface [41,42]. In the case of equaxed WSe_2 nano-grains embedded in amorphous a-WSe_x matrix, WSe_2 nanocrystallites might re-orient themselves in the favor direction normal to the sliding interface as well. Additional study is necessary to clarify this question.

Under water, friction coefficient of WSe_x/TiSiN coating was as low as 0.06 (Fig. 11). The background of friction curve was typically flat, although the fluctuations within the range of 0.04–0.1 were observed. The

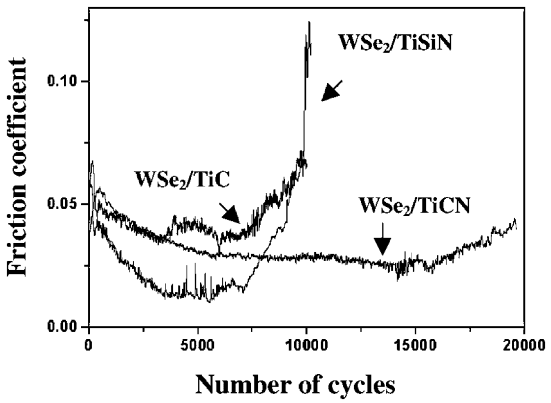

Fig. 10. Friction coefficients of the double-layer coatings against 3-mm WC+6%Co ball.

results obtained show that the WSe_x/TiSiN coatings are effective as lubricants, even under water.

Oxygen is a common contaminant of the transition metal dichalcogenides. The oxygen atoms have been reported to substitute for non-metallic atoms in MoS_2 structure to form $MoS_{2-x}O_x$ and deteriorate friction performance [43]. In contrast, improved WSe_x film performance in our study could be due to film composite structure consisting of WSe_2, W_3O and a-WSe_x phases.

4. Summary

The WSe_x films were formed by PLD and IAPLD. The microstructure and chemical composition of WSe_x films were studied by means of XRD, SEM and TEM, AES and EDS. The WSe_x films were characterized in terms of their hardness, elastic modulus, surface topography and wear performance. The structure of WSe_x films was shown to consist of various nanocrystalline

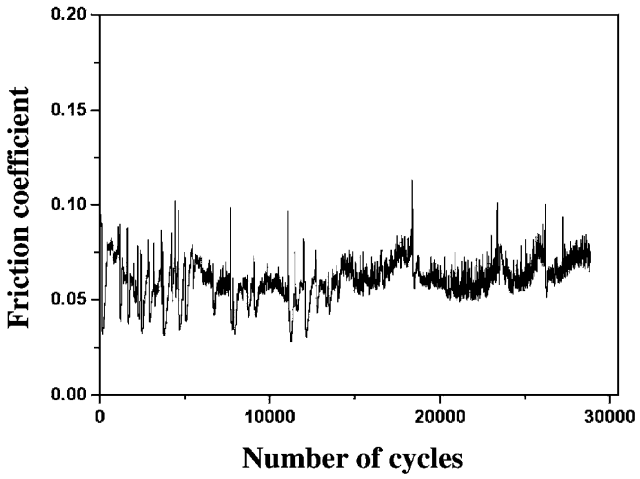

Fig. 11. Friction coefficient of the WSe_x/TiSiN coating against 3-mm WC+6%Co ball under water.

mixtures of WSe_2 and W_3O phases in an a-WSe_x matrix. Depending on deposition conditions, the WSe_2 crystallites were oriented with their basal planes either parallel or perpendicular to the substrate surface. In the last case the incorporation of oxygen atoms between the basal planes caused lattice distortion and increased the *c*-axis lattice parameter. Improved endurance of WSe_x coatings was due to their composite structure. The presence of hard under-layer was shown to be essential for extremely low friction. The WSe_x/TiC films showed low friction from the very start of the tests without initial maximum. The superior performance of WSe_x/hard coating systems both in air and under water suggests that the double-layer coatings are suitable for use in terrestrial tribological applications.

Acknowledgments

The work was fulfilled due to financial support from ISTC, Award No. 1852. We thank D.L. D'yakonov for help with the TEM and Dr N.B. D'yakonova for assistance with XRD experiments.

References

[1] T.P. Molart, J. Haupt, R. Gilmore, W. Gissler, Surf. Coat. Technol. 86–87 (1996) 231.
[2] M. Stüber, H. Leiste, S. Ulrich, H. Holleck, D. Schild, Surf. Coat. Technol. 150 (2002) 218.
[3] K.H. Kim, S. Choi, S. Yoon, Surf. Coat. Technol. 161 (2002) 243.
[4] T. Cselle, A. Barimani, Surf. Coat. Technol. 76–77 (1995) 712.
[5] K.J. Ma, C.L. Chao, D.S. Liu, Y.T. Chen, M.B. Shieh, J. Mater. Proc. Technol. 127 (2002) 182.
[6] D.G. Teer, Wear 251 (2001) 1068.
[7] T.R. Jervis, M. Nastasi, R. Bauer, P.D. Fleischauer, Thin Solid Films 181 (1989) 475.
[8] E. Bergmann, G. Melet, A. Simon-Vermot, Tribol. Int. 14 (1981) 329.
[9] M.S. Donley, J.S. Zabinski, in: D.B. Chrisey, G.K. Hubler (Eds.), Pulsed Laser Deposition of Thin Films, Wiley, New York, 1994, p. 431.
[10] M.S. Donley, P.T. Murray, S.A. Barber, T.W. Haas, Surf. Coat. Technol. 36 (1988) 329.
[11] S.D. Walck, J.S. Zabinski, M.S. Donley, J.E. Bultman, Surf. Coat. Technol. 62 (1993) 412.
[12] V.Yu. Fominski, A.M. Markeev, V.N. Nevolin, Vacuum 42 (1991) 73.
[13] N.T. McDevitt, J.S. Zabinski, M.S. Donley, Thin Solid Films 240 (1994) 76.
[14] V.Yu. Fominski, A.M. Markeev, V.N. Nevolin, V.B. Prokopenko, Thin Solid Films 248 (1994) 240.
[15] S.V. Prasad, J.S. Zabinski, N.T. McDevitt, Tribol. Trans. 38 (1995) 57.
[16] V.Yu. Fominski, V.N. Nevolin, R.I. Romanov, I. Smurov, J. Appl. Phys. 89 (2001) 1449.
[17] M. Hirano, S. Miyake, Appl. Phys. Lett. 47 (1985) 683.
[18] N.J. Mikkelsen, J. Chevallier, G. Sorensen, C.A. Straede, Appl. Phys. Lett. 52 (1988) 1130.
[19] K. Kobs, H. Dimiden, H. Hiibsch, H.J. Tolle, S. Leutenecker, H. Ryssel, Mater. Sci. Eng. 20 (1987) 281.
[20] J.B. Goodenough, Mater. Res. Bull. 3 (1968) 409.
[21] L.C. Upadhyaya, J.J. Lofcrski, A. Wold, J. Appl. Phys. 39 (1968) 4736.
[22] M.K. Agrawal, H.B. Patel, K. Nagirendy, J. Cryst. Growth 60 (1982) 9.
[23] M.S. Simmonds, A. Savan, E. Pflüger, H. Van Swygenhoven, Surf. Coat. Technol. 126 (2000) 15.
[24] V. Fominski, V. Nevolin, R. Romanov, A. Smirnov, V. Titov, W. Scharff, Thin Solid Films 422 (2002) 39.
[25] D.V. Shtansky, I.V. Lyasotsky, N.B. D'yakonova, F.V. Kiryukhantsev-Korneev, S.A. Kulinich, E.A. Levashov, J.J. Moore, Surf. Coat. Technol., in press. **PLEASE UPDATE AT ISSUE STAGE**.
[26] D.V. Shtansky, K. Kaneko, Y. Ikuhara, E.A. Levashov, Surf. Coat. Technol. 148 (2001) 206.
[27] V. Blank, M. Popov, N. Lvova, K. Gogolinsky, V. Reshetov, J. Mater. Res. 12 (1997) 3109.
[28] G.M. Pharr, W.C. Oliver, F.R. Brotzen, J. Mater. Res. 7 (1992) 613.
[29] J. Moser, F. Lévy, Thin Solid Films 240 (1994) 56.
[30] A. Teresiak, G. Weise, N. Mattern, H. Hermann, H.-D. Bauer, Mikrochim. Acta 125 (1997) 349.
[31] D.V. Shtansky, O. Tsuda, Y. Ikuhara, T. Yoshida, Acta Mater. 48 (2000) 3745.
[32] J. Pouzet, J.C. Bernede, A. Khellil, H. Essaidi, S. Benhida, Thin Solid Films 208 (1992) 252.
[33] D.N. Dunn, L.E. Seitzman, I.L. Singer, J. Mater. Res. 12 (1997) 1191.
[34] L.E. Seitzman, R.N. Bolster, I.L. Singer, Thin Solid Films 260 (1995) 143.
[35] R. Collongues, La non-stoechiometrie, Masson et C^{ie} (Editeurs), Paris, 1971, 288 p. (in French).
[36] M.V. Nogenkov, Frict. Wear 8 (1987) 459.
[37] B. Blushan, B.K. Gupta, Handbook of Tribology: Materials, Coatings, and Surface Treatments, McGraw Hill, New York, 1991, p. 5.1, 3.1.
[38] X. Zhang, R. Vitchev, W. Lauwerens, L. Stals, J. He, J.-P. Celis, Thin Solid Films 396 (2001) 69.
[39] M.R. Hilton, G. Jayaram, L.D. Marks, J. Mater. Res. 13 (1998) 1022.
[40] R. Gilmore, M.A. Baker, P.N. Gibson, W. Gissler, M. Stoiber, P. Losbichler, C. Mitterer, Surf. Coat. Technol. 108–109 (1998) 345.
[41] J. Moser, F. Levy, J. Mater. Res. 8 (1993) 206.
[42] J.S. Zabinski, M.S. Donley, S.V. Prasad, N.T. McDevitt, J. Mater. Sci. 29 (1994) 4834.
[43] J.R. Lince, M.R. Hilton, A.S. Bommannavar, Thin Solid Films 264 (1995) 120.